International Journal of Mass Spectrometry 185/186/187 (1999) 673–683

Mass-spectrometric study of formation and stability of manganese and manganese oxide cluster anions

Axel Pramann, Klaus Rademann*

Walther-Nernst-Institut für Physikalische und Theoretische Chemie, Humboldt-Universität zu Berlin, Bunsenstraße 1, 10117 Berlin, Germany

Received 3 July 1998; accepted 23 September 1998

Abstract

We present a mass-spectrometric investigation of the reactions of manganese cluster anions Mn_x^- (in the size range $x = 2–12$) with molecular oxygen in the gas phase. The manganese and manganese oxide cluster anions are studied in a pulsed supersonic molecular beam experiment and generated in a conventional laser vaporization cluster source with an additional flow tube reactor. Relative reactivities are determined at near room temperature as a function of oxygen partial pressure, cluster size, and composition. We observed for the first time the controlled formation of at least four stable manganese oxide series: Mn_xO^-, $Mn_xO_2^-$, $Mn_xO_3^-$, and $Mn_xO_4^-$ ($x = 2–12$). The reactivities decrease rapidly with cluster size reaching a minimum around Mn_4^- and Mn_5^-. They increase smoothly with further increasing cluster size and show no significant pressure dependence for clusters of $x > 5$. The adsorption of molecular oxygen on the cluster surface most probably takes place in a dissociative way resulting in the formation of distinct Mn–O bonds. The Mn_5^- cluster exhibits a special behavior. It has the highest intensity in mass spectra and shows the lowest reactivity towards oxygen. Another interesting feature is the evolution of an intense Mn_2O^- peak with increasing oxygen pressure. (Int J Mass Spectrom 185/186/187 (1999) 673–683) © 1999 Elsevier Science B.V.

Keywords: Clusters; Metal oxides; Manganese; Reactivity; Mass spectrometry

1. Introduction

Over the past decades, cluster science has become an important research area for the investigation of size dependent effects of small aggregates. The goal of these studies is to achieve a better understanding of the situation of chemical bonding and geometric as well as electronic structures. This research also provides new insights into the nature of reaction mechanisms, thermodynamics and kinetics. In particular, transition metal oxides play an important role as catalysts in many fields of industrial chemistry [1,2].

For this reason many scientists have concentrated their research activities on the field of metal and transition metal clusters and its corresponding oxides. These small gas-phase clusters are excellent model systems for reactions in heterogeneous catalysis [3,4]. Clusters represent a useful species because it is well known that the ratio of a number of surface atoms versus the overall number of cluster atoms is very favourable. Therefore, a large active surface on a

* Corresponding author.
Dedicated to Professor Michael T. Bowers on the occasion of his 60th birthday.

PII S1387-3806(98)14197-0

microscopic level is available for catalytic short-range interactions between the incoming reactant and the transition metal oxide substrate.

Since the development of new methods for probing the chemical reactivity of small clusters [5], a lot of work has been devoted to the study of reactions of metal clusters with oxidizing agents in the gas phase [6–14].

In the literature, only few studies of manganese clusters and their compounds in the gas phase have been reported [15]. The production of larger pure manganese clusters in contrast to other transition metal clusters is quite difficult. To understand this phenomenon, one has to focus on the electronic structure of the ground state of the manganese atom, which is a [Ar]$3d^5 4s^2$ configuration. The half-filled $3d$ shell gives the atom a full spherical geometry and high stability. The promotion energy for the $4s^2 3d^5 \rightarrow 4s^1 3d^6$ transition—a necessary process for dimerization—is quite high: 2.14 eV [16]. A limiting factor in the nucleation process is the very low binding energy of the manganese dimer, which is reported to vary from 0.1 ± 0.1 to 0.56 ± 0.26 eV [17–19]. If the dimer is considered as a seeding particle for cluster formation, one also has to emphasize the fact that the electron configuration in the ground state is $(4s\sigma_g)^2(4s\sigma_u^*)^2(3d)^{10}$ and not $(4s\sigma_g)^2(4s\sigma_u^*)^1(3d)^{11}$ [16].

The difficult production of pure manganese clusters is based also on an experimental detail. Because we are interested in showing the evolution of manganese oxide clusters as reaction products starting from Mn_x^- clusters it is important to find both a suitable target material and a cluster source. As already reported by Riley and co-workers [15], α manganese is quite hard and brittle and, of course, very reactive. Therefore, oven- or gas-aggregation techniques produce reaction products as a consequence of high temperatures and cannot be considered as possible cluster sources for our purposes. As reported in detail in sec. 2 we use a purified target rod (99.5% purity) of manganese in a conventional pulsed laser vaporization cluster source.

To our knowledge the use of laser vaporization as a generation method for manganese clusters of both ionic or neutral is rare. Riley and co-workers [15] have applied this source type for studying the nature of the Mn–CH_3 bond and reactions of neutral manganese clusters and carbon-doped manganese clusters with hydrogen. Koretsky and Knickelbein have recently measured photoionization spectra for ionization potential (IP) determination from neutral manganese clusters containing seven up to 64 atoms. They observed a size dependent change in ionization potentials as a consequence of change in cluster geometry [20].

Considerable progress in the field of photoelectron spectroscopy has been made in the group of Kaya and co-workers [21]. They have investigated the electronic structure of small manganese sulfur clusters in the size range of up to 10 manganese atoms. Also the production of alloy clusters containing manganese shows a great challenge for both scientific and industrial knowledge [22]. Binary manganese sulfur cations MnS_y^+ have been probed experimentally by Dance et al. [23]. Saito et al. have succeeded in the observation of magic numbers of positively charged manganese clusters up to 60 atoms with the use of a xenon sputter source [24]. Early reaction studies of catalytic relevance have been reported by Hanley and Anderson using a sputter source [25]. In their work reactions of manganese clusters up to the tetramer with ethylene have been investigated. Gole and co-workers have performed chemiluminescence spectroscopy by probing reactions of manganese vapor with chlorine, fluorine and ozone [26,27]. Additional theoretical studies have been conducted by Weiss et al. on σ-bonding activation in $Mn^+ (H_2)_n$ clusters [28] and by Mackrodt and Williamson about valence states in manganese oxides [29].

Here we present investigations of the controlled formation and stability of small manganese oxide cluster anions $Mn_xO_y^-$ in the size range $x = 2$–12 and $y = 1$–4 using a chemical probe experiment. To the best of our knowledge this is the first investigation concerning manganese oxide cluster anions in the gas phase.

One very stimulating work reported by Ziemann and Castleman [30] is a mass-spectrometric study of cationic $(MnO)_x^+ - (x = 1$–$13)$ and $(MnO)_xO^+$ clusters ($x = 4$–22) generated via gas aggregation. These oxide cluster cations show a quite different

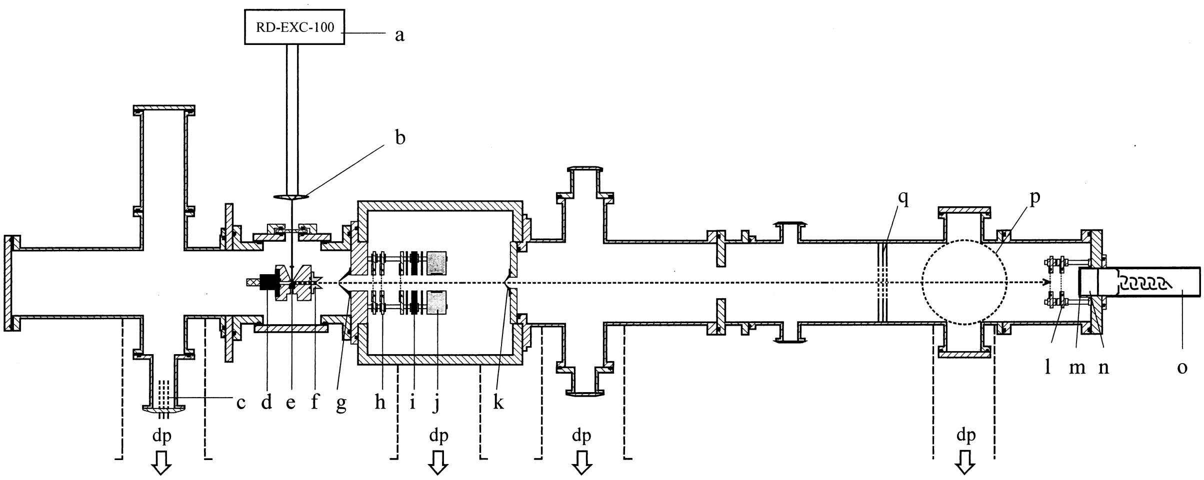

Fig. 1. Molecular beam apparatus (topview cross section). (a) Vaporization laser (308 nm XeCl, 120 mJ/pulse); (b) collimation lens ($f = 300$ mm); (c) ionization gauge; (d) pulsed solenoid valve; (e) target rod; (f) nozzle with conical extender; (g) skimmer; (h) acceleration optics; (i) einzel lens; (j) x/y deflection plates; (k) skimmer; (l) conversion dynode grid; (m) organic scintillator (Al coated); (n) plexi glass light guide; (o) photomultiplier; (p) detector chamber; (q) three-grid mass gate; dp: diffusion pump.

formation pattern than observed for negatively charged oxides in this work as will be discussed in the following sections.

2. Experimental

In the present article we describe our new molecular beam apparatus in detail. A schematic of the entire apparatus is shown in Fig. 1.

The apparatus is a four-chamber-type linear molecular beam machine. The generation and further spectroscopic study (mass spectrometry and other spectroscopic techniques) of unperturbed clusters in the gas phase require the production of intense cold noninteracting clusters in either a continuous or a pulsed mode. For several reasons, we use a pulsed design. First, in a pulsed mode smaller pumps can maintain the vacua. Another advantage is a low consumption rate of material (gas, target). The most important reason is the availability of pulsed lasers, coupled with a pulsed cluster source.

The first chamber (see Fig. 1 from left to right) contains the cluster source and the flow tube reactor (not shown in Fig. 1). The clusters undergo an adiabatic supersonic expansion to form translationally cold beam bunches and enter the second chamber containing the acceleration optics, deflection plates and an einzel lens of the time-of-flight mass spectrometer. Subsequently, the clusters enter a third chamber (acting as a drift zone). The detector of the mass spectrometer is mounted at the end of the last chamber. Also in this chamber further spectroscopic experiments are planned perpendicular to the molecular beam using a mass gate for the selection of appropriate ions. The in-line design of the apparatus is selected to gain high intensities for spectroscopic investigations. All chambers are pumped via well-baffeled oil diffusion high vacuum pumps. In pulsed operation without reactive gas addition the pressure is in the range of 8×10^{-5} mbar in the source chamber to 8×10^{-7} mbar in the detection chamber. When the reactive gas is added into the flow tube reactor, the pressure in the source chamber rises to 8×10^{-4} mbar.

2.1. Cluster generation

For cluster generation we use a conventional laser vaporization cluster source based on the pioneering work of Smalley and co-workers [31–33], Bondybey and English [34] and Milani and de Heer [35,36].

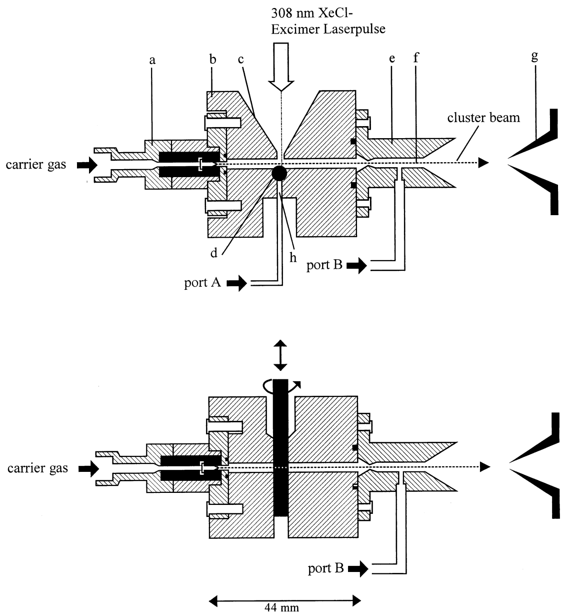

Fig. 2. Upper part: horizontal cross section of the pulsed laser vaporization cluster source (a) pulsed solenoid valve (General Valve Corp. Series 9), (b) stainless steel source body, (c) conical channel: vaporization laser entrance, (d) target rod (3 mm diam.), (e) fast flow tube reactor (extender, reactive gas inlet: port B), (f) reaction channel, (g) stainless steel skimmer, (h) second gas inlet (port A) and vaporization light adjusting channel. Lower part: side cross section of the pulsed laser vaporization cluster source; the dashed line denotes the carrier gas flow, respectively the cluster beam.

Fig. 2 shows a schematic of the cluster source. The upper part is a horizontal cross section with the dashed line showing the flow of the cluster beam whereas the lower part is a side cross section of the pulsed laser vaporization cluster source.

The black circle in the center is a 2.5 mm diameter manganese target rod (30 mm in length) with a purity of 99.5% (Goodfellow). The source body made of stainless steel is equipped with a nucleation channel (2 mm in diameter, 20 mm in length), a fast pulsed solenoid valve (General Valve Corp. Series 9) with a 0.5 mm nozzle and a flow tube reactor (described in Sec. 2.2). The whole source is mounted in each *xyz* direction to adjust both the source nozzle and the vaporization laser.

Perpendicular to the nucleation channel a pulse of a 308 nm XeCl excimer laser (120 mJ pulse energy, 25 ns pulse width; Radiant Dyes Acc.) is focused onto the rotating translating target rod via a 300 mm LiF lens. The resulting plasma is thermalized in the clustering channel with a high-pressure helium carrier gas pulse (12 bar, 400 μs duration). In this work helium with a purity of 99.999% is used (Messer Griesheim). The firing of the vaporization laser is carefully adjusted on the leading edge of the helium pulse to produce high intensities of translationally cold clusters. A very critical parameter is the time delay between the firing of the vaporization laser and the opening of the pulsed valve. In the case of manganese clustering is occurring only within a short delay bandwidth of about 20 μs (other metals: 100 μs). We use a conical entrance channel for the vaporization laser light in order to make the laser adjustment much easier. The vaporization laser light is focused onto the detector directed side of the target rod to ensure the complete portion of the metal plasma being expanded towards the source nozzle. Behind the target rod the light adjusting channel (h in Fig. 2) is supplied with a thread. So a second gas inlet (port A, not used in this work) is available.

The typical repetition rate of the experiment is about 5–7 Hz limited by the gas load.

2.2. Reactivity experiments

The reactivity experiments reported in this work are carried out in a fast flow reactor [5,37].

After formation the cluster bunch expands through a first nozzle with an orifice of 1 mm in diameter. Passing this nozzle the clusters enter the flow tube reactor channel (20 mm in length, 2 mm in diameter) made of stainless steel. In the center of this tube a gas inlet (port B in Fig. 2) with a one mm orifice is located. The oxydizing gas (in this work: O_2 with 99.995% purity, Messer Griesheim) is added through this port causing a turbulent mixing which will ensure a sufficient contact of the reactants.

After reaction the clusters undergo an adiabatic supersonic beam expansion. A conical extender at the end of the reaction channel ensures a directed cold cluster beam with high intensity. In a distance of 2 cm a stainless steel skimmer (2 mm orifice, 60° outer angle, 40° inner angle) forms a well collimated beam and separates the source chamber from the acceleration chamber.

The oxygen is added continuously through port B (oxygen pressure: 1.00–3.70 mbar) in steps of roughly 0.5 mbar. In order to achieve a very stable flow of oxygen a series of three microinlet valves is used. All gas lines are purified and baked out before every series of measurements. The continuous addition of oxygen has no significant effect concerning the pressure in the first chamber, which is pumped by a 3800 L/s diffusion pump (0.5 m in diameter) backed with a roots blower (97 L/s).

The 1 mm nozzle located between the clustering channel and the reaction channel is producing an oxygen flow directed mainly towards the skimmer and not towards the target rod as a consequence of the pressure gradient. Also the high abundance of Mn_x^- clusters in mass spectra of oxide clusters show that mainly metal clusters are formed before colliding with the reactant gas. Only a small amount of oxygen is present in the plasma around the target. This has been proven by oxide formation after adding a trace of O_2 to the helium carrier gas: Mn_x^- peaks are strongly suppressed and oxide peaks are by two orders of magnitude more intensive than in the case of flow tube reactions. The temperature in the nucleation channel cannot be measured and is estimated to about 300 ± 25 K [37] (we are working in a pulsed mode [37–39]). The overall pressure in the nucleation channel is calculated by means of gas dynamics to 3 ± 2 bar. The oxygen partial pressure is measured with a pirani gauge located near the gas inlet (port B).

Therefore, we are not able to determine absolute rate constants, but it is possible to monitor the reactivity pattern as a function of O_2 partial pressure.

Relative reactivities $R_{x,y}$ are determined with the expression

$$R_{x,y} = \frac{I_{Mn_xO_y^-}}{I_{Mn_x^-}} \tag{1}$$

$I_{Mn_xO_y^-}$ is the intensity of the xth manganese oxide cluster of interest after oxygen addition and $I_{Mn_x^-}$ is the intensity of the corresponding pure manganese cluster Mn_x^- in the same mass spectrum. Since absolute intensities of mass peaks differ in a short range between many measurements it is not useful to determine $I_{Mn_x^-}$ from a separate reference spectrum with pure undepleted manganese clusters. Therefore, our $R_{x,y}$ ratios are related to one and the same mass spectrum to guarantee a high accuracy of formation conditions. Each reactivity pattern is found to be quite reproducible during a variety of measurements. Thus, we are able to postulate pressure dependent reactivities as will be shown in Sec. 2.3.

2.3. Mass analysis

In this work all measurements are carried out with the aid of a conventional time-of-flight mass spectrometer (TOF-MS) of the Wiley/McLaren design [40]. Even if the mass resolution (in our case: $m/\Delta m = 60$) is not as large as is achieved with other kinds of mass spectrometric techniques a TOF-MS shows a list of advantages. First of all the mass range is not limited. Also a complete mass spectrum can be recorded at a single event. Different masses of cluster ions are separated according to their mass-to-charge ratios. In a first acceleration field negatively charged clusters are pulsed towards a second acceleration field. Subsequently bunches of cluster ions with the same kinetic energy are separated due to different velocities, and mass, respectively, in a linear drift tube of 1 m in length. The two acceleration fields are constructed of CrNi meshes of high transmittance. Pulsed voltages of -1770 and -1550 V (10–40 μs duration) are applied to these grids by fast high voltage switches (Behlke, HTS 31). The entire pulse correlation is maintained with pulse/delay generators (Stanford Research Systems DG 535).

In this work a newly developed in-line anion detector of a modified Daly-type [41] (see Fig. 1 for details) is used.

It consists of a first electrode grid (CrNi-mesh, 80% transmission) at ground potential, a second electrode at $+2$ kV (l in Fig. 1) and an Al-coated organic scintillator ($+14$ kV) coupled to a photomultiplier (R 329-02, Hamamatsu) via a Plexiglas light guide. The detected secondary electrons are emitted from the second grid which has the function of a "conversion dynode" known from the Daly detector.

The signals are accumulated, averaged (1000–2000 shots each spectrum) and stored by a digital oscilloscope (LeCroy DSO 9361) without further amplification and transferred to a personal computer.

3. Results and discussion

In this section we present reactivity experiments of manganese cluster anions with the dioxygen molecule in the gas-phase.

It is necessary to start with the formation of manganese cluster anions Mn_x^- in order to demonstrate the evolution of metal oxide cluster anions as a function of both oxygen concentration, number of manganese atoms and cluster composition. We explain the evolution of oxide clusters in terms of valence electron behavior and discuss the question whether the oxygen chemisorption is dissociative or molecular. Furthermore the abundance of some prominent peaks, especially the Mn_5^- ion is discussed. Finally, the pressure dependence of the relative reactivities is analyzed in terms of probable fragmentation channels after collision of manganese oxides with a surplus of dioxygen in the reaction tube.

3.1. Mn_x^--clusters

Fig. 3 shows a typical time-of-flight spectrum of Mn_x^- in the size range $x = 3–16$. Generally, some satellite peaks occur (see the peaks to the left and right of Mn_x^-). These mass peaks are related to small $Mn_xCH_y^-$ anions (carrier gas impurities, pumping oil) and MnC^- impurities (traces of carbon in the target). The strong CH_x affinity of manganese is explained by a large Mn–CH_x binding energy, which has been proved by the reaction of manganese and manganese carbides with hydrogen [15]. There the Mn–CH_3 bond has been determined to 1.21 ± 0.09 eV. The series of pure manganese cluster anions starts with the (dimer or (in Fig. 3) with the trimer). The absence of the

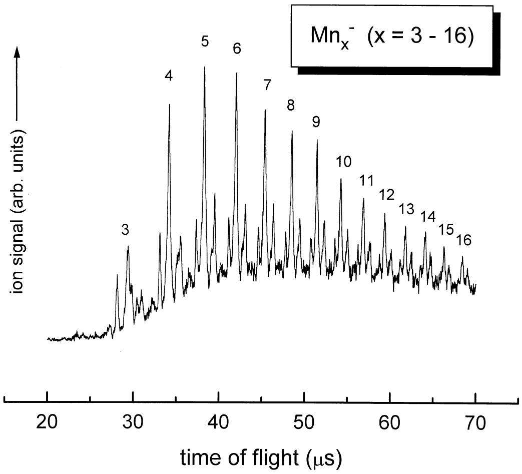

Fig. 3. Mass spectrum of Mn_x^--clusters ($x = 3–16$).

monomer is a result of a negative electron affinity (EA). Nishio et al. [42] have measured electron affinities of Mn_x with $x = 2–4$ and postulated a negative EA of the monomer. Although Riley and co-workers [15] could observe significant amounts of Mn_x^+ cations only by using a cryogenic laser vaporization cluster source we are able to produce small negatively charged manganese clusters at near room temperature. This "room temperature" formation might be a consequence of the precise timing of the laser pulse versus the maximum of the carrier gas pulse. We also apply a carrier gas density as high as possible to permit a very efficient temperature relaxation of the clusters. Of course, in comparison with other transition metal cluster anions produced with our apparatus (e.g. Au, Ag, Cu) the absolute intensities in the case of manganese are by two orders of magnitude lower. This fact corresponds to the difficult formation of these aggregates. Unfortunately, when treating *d* elements the use of shell models is quite ineffective due to the large number of energetically low lying *d* electrons. So it is difficult to correlate the presence of magic numbers with special electronic structures. The manganese anion possesses eight valence electrons in its respective ground state. Therefore, shell closings are rather improbable using potentials like the square well or the harmonic oscillator.

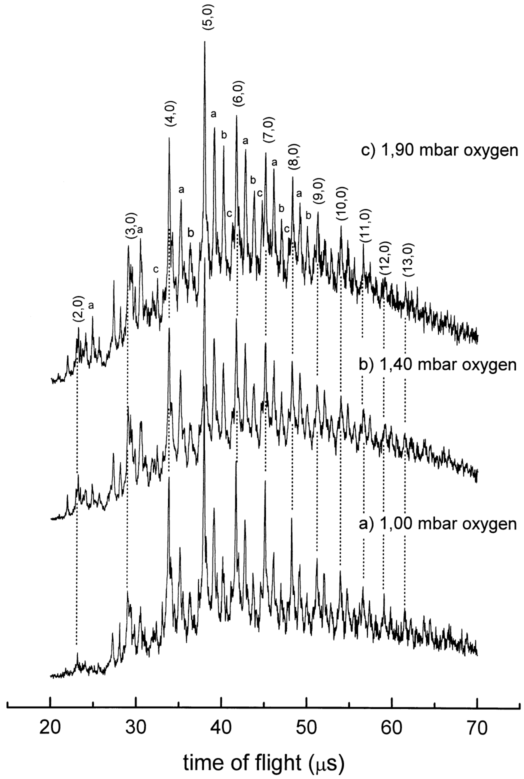

Fig. 4. (a)–(c) Evolution of manganese oxide cluster anion series with increasing oxygen partial pressure. Note the dominating Mn_5^--peak. *a*, *b*, *c* correspond to each monoxide, dioxide and trioxide of the *x*th cluster.

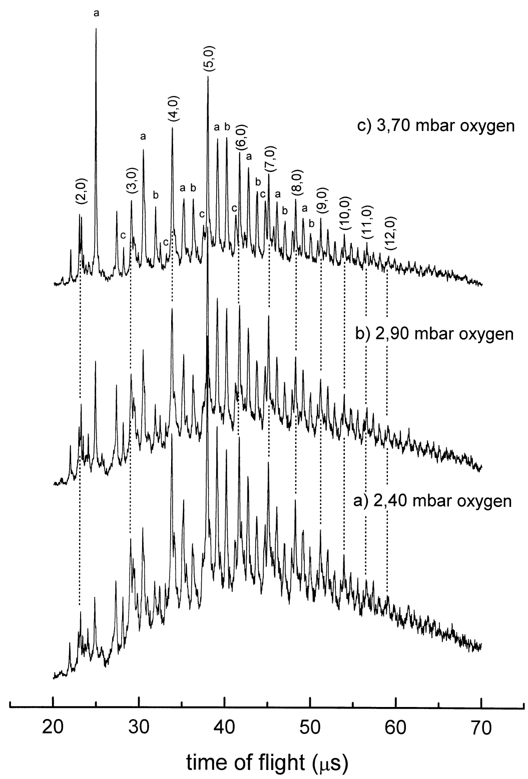

Fig. 5. (a)–(c) Manganese oxide cluster anions after increase of oxygen partial pressure. When reaching the 3.70 mbar limit the Mn_2O^--peak dominates the entire spectrum.

3.2. Manganese oxide cluster anions

We observed the controlled formation of manganese oxide cluster anion series as a function of oxygen pressure: Mn_aO^- ($a = 2$–12), $Mn_bO_2^-$ ($b = 3$–12), $Mn_cO_3^-$ ($c = 2$–12), and less intense $Mn_dO_4^-$ ($d =$ 2–11). For simplification the indices a, b, c, d are replaced in the following by the index x ($Mn_xO_y^-$ clusters).

During all measurements the $Mn_2O_2^-$ ion has never been observed. The manganese oxide mass spectra are shown in Figs. 4–6.

At a first glance, the mass spectra shown in Figs. 4–6 indicate that manganese cluster anions readily react with the dioxygen molecule. The following formation pattern of most metal oxides is observed: Every Mn_x^- mass peak is accompanied by a series (at higher oxygen pressures: triplets) of oxide peaks. The first peak corresponds to the monoxide, the second belongs to the dioxide and the third is the trioxide. A more precise analysis shows that also $Mn_xO_4^-$-clusters are formed, but the latter are always very weak in intensity.

Generally, the absolute intensities of the Mn_x^- peaks decrease with increasing oxygen partial pressure, but the intensity of the xth element peak is always larger than the intensities of the corresponding oxide clusters for $x \geq 3$. Smaller clusters (the dimer and trimer, respectively) show a rather different behavior of intensity distributions as will be discussed later.

We have measured highly reproducible metal oxide spectra at 1.00, 1.40, 1.90, 2.40, 2.90, and 3.70 mbar oxygen pressure (see Figs. 4–6). At oxygen pressures around 1.00 mbar the mass spectrum is

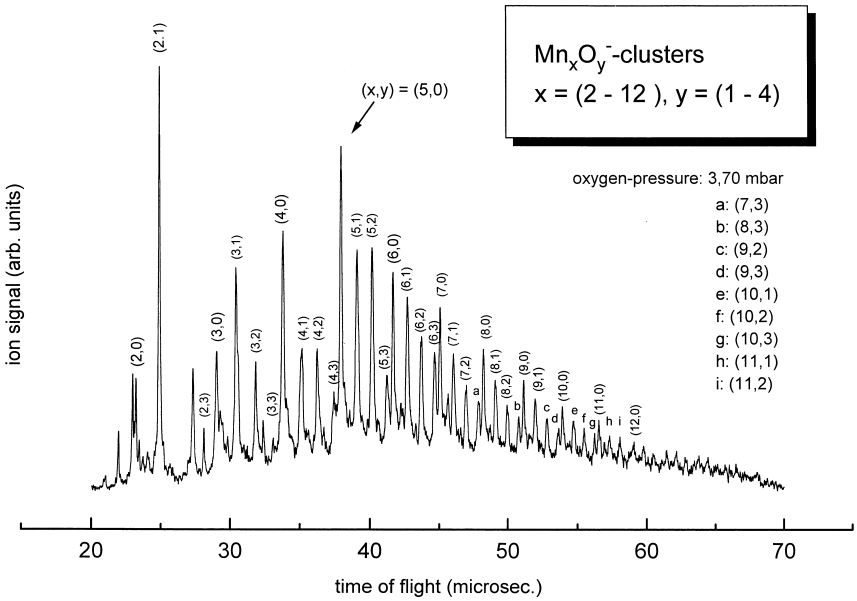

Fig. 6. Detailed mass spectrum of $Mn_xO_y^-$ obtained when 3.70 mbar oxygen is added.

dominated by the pure Mn_x^- clusters with $x = 4$–8. The respective monoxide Mn_xO^- is clearly formed with high abundance followed by the dioxide $Mn_xO_2^-$. This pattern is observed for $x > 3$. Increasing the oxygen pressure to 1.40 and 1.90 mbar the triplet series of the first three oxides evolves as a more and more clear feature. Every spectrum is dominated by the intense manganese pentamer anion located in the center of the mass distribution.

If the oxygen pressure is further increased the evolution of a new oxide peak can be monitored. Unexpectedly, this Mn_2O^- peak becomes the dominating peak in the 3.70 mbar spectrum.

An open question regarding the four manganese oxide series is the kind of bonding between manganese and each set of oxygens. It is well known that transition metal surfaces will adsorb the dioxygen molecule *dissociatively* when chemisorption conditions at near room temperature (or above) are considered. Taking a look at the stoichiometry of the manganese oxides, the monoxide always shows a high abundance. So in general, even if we cannot exclude a molecular chemisorption at all, the strong formation of the odd numbered monoxide and trioxide is an indication for dissociative chemisorption. Another reason for dissociative chemisorption is a larger binding energy of atomically adsorbed species on the cluster surface. A large oxygen–manganese bond strength is necessary since every oxide cluster collides many times with the carrier gas atoms and dioxygen molecules. Therefore, desorption effects are avoided only by strong chemical bonding between oxygen and manganese. Regarding electronic effects of chemisorption one has to take into consideration that the highest occupied molecular orbital of O_2 is a π^* antibonding orbital and a transfer of electron density from the metal towards these antibonding orbitals will weaken the O–O bond. So, a cleavage of the dioxygen bond will occur.

In all six oxygen pressure ranges the relative reactivities of the xth manganese cluster towards molecular oxygen have been determined using Eq. (1). Fig. 7 shows the measured relative reactivities as a function of manganese atoms per cluster (x) at 3.70 mbar O_2 partial pressure.

Some general trends in the reactivity of negatively charged manganese clusters are observed independently which oxygen pressure has been applied.

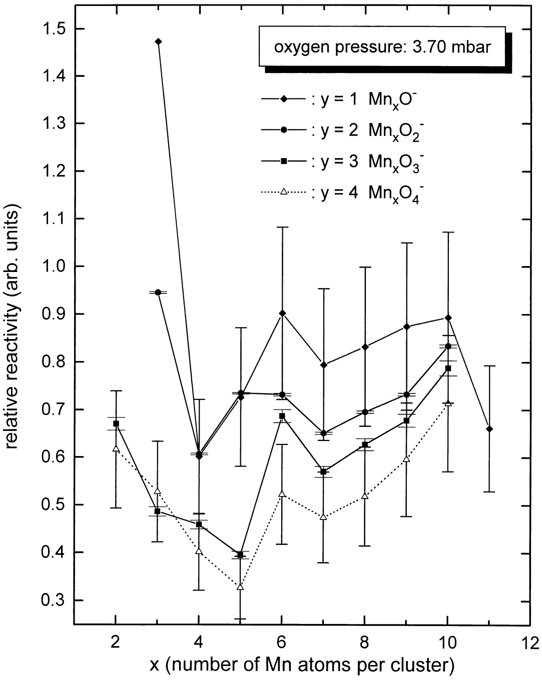

Fig. 7. Relative reactivity $R_{x,y}$ as a function of cluster size at 3.70 mbar oxygen partial pressure.

Comparing the four oxide series the following sequence in $R_{x,y}$ is determined: $Mn_xO^- > Mn_xO_2^- > Mn_xO_3^- > Mn_xO_4^-$ (the absolute intensity is decreasing in the same order). Relative reactivities decrease from the dimer to the tetramer and pentamer by about one order of magnitude (especially when starting with Mn_2O^-). The minimum of relative reactivities is located around the tetramer and pentamer for each oxygen pressure and also for each oxide series corresponding to the high intensities of the Mn_4^- and Mn_5^- ions. After this drop the reactivity is increasing with increasing cluster size.

The alternations in $R_{x,y}$ for $x > 5$ show no regular pattern and do not follow even/odd alternations in cluster size.

The weak increase in reactivity with cluster size ($x > 5$) for each oxide series might be a consequence of *surface saturation* effects. If a larger active surface is available the reaction probability is enhanced. Regarding the mass spectra (Figs. 4–6) it is evident that with increasing O_2 partial pressure the intensity of higher series ($y = 3, 4$) increases.

Another feature is the strongly increasing peak intensity of Mn_2O^- when exceeding a limit of about 1.90 mbar dioxygen partial pressure. The relative reactivity of this monoxide is larger than 1 at 1.90 mbar and in the 3.70 mbar plot out of range ($R_{x,y} = 3.07$). The Mn_3O^- peak shows a similar behavior. What are the reasons for this increasing intensity of these very small monoxides when coming to higher pressures? We assume that the formation of Mn_3O^- and especially of Mn_2O^- is not only a consequence of direct oxygen chemisorption of initially abundant Mn_3^- and Mn_2^- clusters, but might also be a result of collision induced fragmentation of larger clusters. Probable fragmentation channels are:

$$Mn_xO_y^- + O_2 \rightarrow \mathbf{Mn_2O^-} + \text{other products}$$

$$Mn_x^- + O_2 \rightarrow \mathbf{Mn_2O^-} + \text{other products}$$

and less efficient

$$Mn_xO_y^- + O_2 \rightarrow \mathbf{Mn_3O^-} + \text{other products}$$

$$Mn_x^- + O_2 \rightarrow \mathbf{Mn_3O^-} + \text{other products}$$

with $x \gg 2$.

Of course, this is quite speculative and must be proved by further studies. Nevertheless a fragmentation according to this scheme is much more probable than direct reaction of the dimer and trimer with molecular oxygen when analyzing the pressure dependence: When an excess amount of the dioxygen molecule (here: 3.70 mbar) is present in the reaction channel the initially formed larger Mn_x^- clusters will fragment after many collisions with O_2. Then smaller fragments like Mn_2^- and Mn_3^- react readily with oxygen. Another way is the initial formation of larger $Mn_xO_y^-$ species which will be reheated after adsorption of oxygen. This additional remaining energy will deplete the large oxide clusters, because the excess energy cannot be carried away efficiently by the carrier gas in the presence of higher O_2 pressures.

3.3. The pentamer: Mn_5^-

Analyzing both mass spectra and reactivity behavior it is obvious that the pentamer Mn_5^- might be treated as a "magic number." The pentamer peak is the most prominent in each mass spectrum (except the Mn_2O^- peak) with or without the addition of oxygen and marks the center of a Gaussian-like intensity distribution. With few exceptions the pentamer exhibits for every pressure regime a local minimum in relative reactivity $R_{x,y}$ toward O_2. This clearly demonstrates the high stability of the Mn_5^- cluster and its low reactivity towards the dioxygen molecule at near room temperature compared with neighbouring cluster sizes. This behavior occurs independently whether the oxygen pressure increases or not. Now the question arises: Why is the pentamer such a stable species? Considering electronic effects Mn_5^- has 36 valence electrons. Applying conventional shell models there is no indication of a shell closing. Unfortunately, electron affinities of manganese clusters larger than the tetramer have not been measured [42]. It is important that in the case of cations Mn_x^+ the pentamer is also found to be a magic number. Both Sone et al. [22] and Saito et al. [24] have found this behavior though they have used quite different cluster sources. It might be concluded that the stability of the pentamer is the result of a geometric effect. The geometric structures (isomers) of the pentamer should therefore be very stable independently whether the charge is positive or negative. Van Zee et al. [43] have shown by the aid of electron spin resonance experiments on matrix isolated neutral Mn_5 clusters that the pentamer has the structure of a planar pentagon. If this structure could be transferred to gas phase clusters or not can only be clarified by combining both spectroscopy and theory.

4. Conclusion

This study shows that small manganese cluster anions in the gas-phase react readily with molecular oxygen as a consequence of available *d* electrons. As in the case of other transition metal clusters the reaction is explained in terms of dissociative chemisorption mechanisms resulting in a variety of nonstoichiometric oxides starting with the monoxide followed by a stepwise addition of single oxygen atoms. A weak increase in reactivity of manganese clusters with increasing oxygen pressure is observed. At higher oxygen pressures we assume a dominant collision induced fragmentation channel resulting in the formation of the Mn_2O^- molecule. Another result is the very stable character of Mn_5^-, which is explained by a strong geometric effect.

These studies will help to understand macroscopic effects in surface reactions which are of considerable importance in the development of more active and selective heterogeneous catalysts.

To get a deeper insight into reactivity patterns more experimental work in screening the reactivity behavior and the electronic structure is in preparation. It would be also very helpful if theoretical studies will support experimental work in the near future.

Acknowledgements

The authors thank Dr. Ourania Dimopoulou-Rademann for many fruitful discussions. Financial support by the Fonds der Chemischen Industrie and by the Humboldt-Forschungs fond is gratefully acknowledged.

References

[1] H.H. Kung, Transition Metal Oxides—Surface Chemistry and Catalysis, Elsevier, New York, 1989.
[2] V.E. Henrich, P.A. Cox, The Surface Science of Metal Oxides, Cambridge University Press, New York, 1994.
[3] P. Schnabel, K.G. Weil, M.P. Irion, Angew. Chem. 104 (1992) 633.
[4] Y. Shi, K.M. Ervin, J. Chem. Phys. 108 (1998) 1757.
[5] See for example: P.S. Bechthold, E.K. Parks, B.H. Weiller, L.G. Pobo, S.J. Riley, Zeitschr. f. Phys. Chem. N. F. 169 (1990) 101, and references therein.
[6] D.M. Cox, D.J. Trevor, R.L. Whetten, A. Kaldor, J. Phys. Chem. 92 (1988) 421.
[7] R.E. Leuchtner, A.C. Harms, A.W. Castleman Jr., J. Chem. Phys. 91 (1989) 2753.
[8] M.R. France, J.W. Buchanan, J.C. Robinson, S.H. Pullins, J.L. Tucker, R.B. King, M.A. Duncan, J. Phys. Chem. A 101 (1997) 6214.
[9] M. Kinne, T.M. Bernhardt, B. Kaiser, K. Rademann, Int. J. Mass Spectrom. Ion Processes 167/168 (1997) 161.
[10] W.D. Vann, R.L. Wagner, A.W. Castleman Jr., J. Phys. Chem. A 102 (1998) 1708.

[11] R.C. Bell, K.A. Zemski, K.P. Kerns, H.T. Deng, A.W. Castleman Jr., J. Phys. Chem. A 102 (1998) 1733.
[12] J.B. Griffin, P.B. Armentrout, J. Chem. Phys. 106 (1997) 4448.
[13] T.H. Lee, K.M. Ervin, J. Phys. Chem. 98 (1994) 10023.
[14] P.A. Hintz, K.M. Ervin, J. Chem. Phys. 103 (1995) 7897.
[15] E.K. Parks, G.C. Nieman, S.J. Riley, J. Chem. Phys. 104 (1996) 3531.
[16] M.F. Jarrold, in H. Haberland (Ed.), Cluster of Atoms and Molecules Vol. I, Springer, New York, 1994, p. 326.
[17] K. Ervin, S.K. Loh, N. Aristov, P.B. Armentrout, J. Phys. Chem. 87 (1983) 3593.
[18] A. Kant, S.-S. Lin, B. Strauss, J. Chem. Phys. 49 (1968) 1983.
[19] M.D. Morse, Chem. Rev. 86 (1986) 1049.
[20] G.M. Koretsky, M.B. Knickelbein, J. Chem. Phys. 106 (1997) 9810.
[21] N. Zhang, H. Kawamata, A. Nakajima, K. Kaya, J. Chem. Phys. 104 (1996) 36.
[22] Y. Sone, K. Hoshino, T. Naganuma, A. Nakajima, K. Kaya, J. Phys. Chem. 95 (1991) 6830.
[23] I. Dance, K. Fisher, G. Willett, Angew. Chem. 107 (1995) 215.
[24] Y. Saito, H. Ito, I. Katakuse, Z. Phys. D 19 (1991) 189.
[25] L. Hanley, S.L. Anderson, Chem. Phys. Lett. 122 (1985) 410.
[26] T.C. Devore, J.R. Woodward, J.L. Gole, J. Phys. Chem. 93 (1989) 4920.
[27] T.C. Devore, J.L. Gole, J. Phys. Chem. 100 (1996) 5660.
[28] P. Weis, P.R. Kemper, M.T. Bowers, J. Phys. Chem. A 101 (1997) 2809.
[29] W.C. Mackrodt, E.-A. Williamson, Ber. Bunsenges. Phys. Chem. 101 (1997) 1215.
[30] P.J. Ziemann, A.W. Castleman Jr., Phys. Rev. B 46 (1992) 13480.
[31] T.G. Dietz, M.A. Duncan, D.E. Powers, R.E. Smalley, J. Chem. Phys. 74 (1981) 6511.
[32] D.E. Powers, S.G. Hansen, M.E. Geusic, A.C. Pulu, J.B. Hopkins, T.G. Dietz, M.A. Duncan, P.R.R. Langridge-Smith, R.E. Smalley, J. Phys. Chem. 86 (1982) 2556.
[33] S. Maruyama, L.R. Anderson, R.E. Smalley, Rev. Sci. Instrum. 61 (1990) 3686.
[34] V.E. Bondybey, J.H. English, J. Chem. Phys. 74 (1981) 6978.
[35] P. Milani, W.A. de Heer, Rev. Sci. Instrum. 61 (1990) 1835.
[36] W.A. de Heer, P. Milani, Z. Phys. D 20 (1991) 437.
[37] M.E. Geusic, M.D. Morse, S.C. O'Brian, R.E. Smalley, Rev. Sci. Instrum. 56 (1985) 2123.
[38] (a) M.D. Morse, M.E. Geusic, J.R. Heath, R.E. Smalley, J. Chem. Phys. 83 (1985) 2293; (b) M.E. Geusic, M.D. Morse, R.E. Smalley, ibid. 82 (1985) 590.
[39] (a) M.R. Zakin, R.O. Brickman, D.M. Cox, A. Kaldor, J. Chem. Phys. 88 (1988) 6605; (b) 88 (1988) 3555.
[40] W.C. Wiley, I.H. McLaren, Rev. Sci. Instrum. 26 (1955) 1150.
[41] N.R. Daly, Rev. Sci. Instrum. 31 (1960) 264.
[42] T. Nishio, J. Matsumoto, K. Takahashi, M. Ichihashi, A. Terasaki, M. Tsukada, T. Kondow, Book of Abstracts, International Symposium on Small Particles and Inorganic Clusters ISSPIC 8, 1996, p. 1.16.
[43] (a) R.J. Van Zee, C.A. Baumann, S.V. Bhat, W. Weltner Jr., J. Chem. Phys. 76 (1982) 5636; (b) C.A. Baumann, R.J. Van Zee, S.V. Bhat, W. Weltner Jr., ibid. 78 (1983) 190.